Journal of Integrative Neuroscience

J. Integr. Neurosci. **2026**; 25(2): 47749
https://doi.org/10.31083/JIN47749

Original Research

Draxin Induces Cognitive Impairment in Mice via Wnt/β-Catenin-Mediated Tau Phosphorylation

Qingcheng Chen[1,†], Yiwei Fu[1,†], Li Hu[1,2], Xiaoxia Chen[1], Zhou Liu[1,*]

[1]Guangdong Key Laboratory of Age-Related Cardiac and Cerebral Diseases, Department of Neurology, Institute of Neurology, Affiliated Hospital of Guangdong Medical University, 524000 Zhanjiang, Guangdong, China
[2]School of Basic Medical Sciences, Guangdong Medical University, 524000 Zhanjiang, Guangdong, China
*Correspondence: liuzhou@gdmu.edu.cn (Zhou Liu)
[†]These authors contributed equally.
Academic Editor: Gernot Riedel
Submitted: 28 October 2025 Revised: 15 December 2025 Accepted: 18 December 2025 Published: 6 February 2026

Abstract

Background: Dorsal repellent axon guidance protein (draxin) is a secreted protein that plays an establishment role in the formation of proper connections between neurons. Although draxin is known to regulate the elongation of axons from various types of neurons *in vitro*, its specific role in mature neurons remains unclear. Draxin expression in the hippocampal region of patients with Alzheimer's disease (AD) has been reported to be higher than in normal subjects. The present study investigated the effect of draxin on the expression of microtubule-associated protein 2 (MAP2) and neuronal nuclear antigen (NeuN), and on tau protein phosphorylation in mouse hippocampal neurons (HT22 cells) and AD cellular models. In addition, stereotactic techniques were used to inject neuronal-targeted adeno-associated virus (AAV) into the hippocampus of C57BL/6 mice to assess the effects of draxin overexpression on hippocampal neurons, as well as on behavioral and pathological features. **Methods**: *In vitro* experiments were conducted using mouse hippocampal neuronal cells (HT22 cells) and established AD cellular models, focusing on evaluating draxin's effects on the expression of neuronal markers (MAP2 and NeuN) and the phosphorylation status of tau protein. For *in vivo* validation, neuron-targeted AAV was delivered into the hippocampus of C57BL/6 mice via brain stereotactic injection to achieve draxin overexpression. Subsequent assessments included analyses of hippocampal neuronal integrity, behavioral tests (Y-maze and Morris water maze, to evaluate spatial learning and memory), and detection of AD-related pathological markers. **Results**: *In vitro* experiments revealed that draxin overexpression decreased the cell survival rate, increased the apoptosis rate, decreased the expression of MAP2 and NeuN, and showed a trend for increased phosphorylation of tau protein compared with the control group. Notably, the spatial learning memory ability of mice with draxin overexpression in the brain, as determined by the Y-maze and Morris water maze tests, was significantly diminished compared with the control group. These mice also showed elevated tau protein phosphorylation and altered expression of wingless-related integration site (Wnt)/β-catenin/glycogen Synthase Kinase 3 beta (GSK-3β) pathway components. **Conclusions**: Our results suggest for the first time that neuronal overexpression of draxin may induce neuronal damage via the Wnt/β-catenin/GSK-3β signaling pathway, leading to AD-like neuropathological damage and cognitive dysfunction.

Keywords: draxin; hippocampal neurons; cognitive dysfunction; Alzheimer's disease

1. Introduction

Alzheimer's disease (AD) is a neurodegenerative disease characterized by progressive cognitive dysfunction. The main characteristic pathological changes of AD are senile plaques formed by extracellular amyloid-β (Aβ) and neurofibrillary tangles (NFTs) formed by aggregates of phosphorylated tau (p-tau) [1], leading to neuronal dysfunction and ultimately to cognitive decline. The rate of neurogenesis declines during adulthood and aging [2–4]. Moreover, adult hippocampal neurogenesis is significantly reduced in AD patients and murine models of AD [5,6]. The expression of neurogenesis-associated genes, including doublecortin (DCX) and sex-determining region Y-box 2 (Sox2), is reduced in patients with severe AD compared with early AD patients and non-demented controls, possibly impairing hippocampal neurogenesis [3,7–9].

Dorsal inhibitory axon guidance protein (Draxin) is a secreted protein involved in axon guidance and the development of the forebrain and dorsal spinal cord [10–12]. Recent studies suggest that draxin may also be involved in the regulation of mature neurons. For example, draxin protein [13] can be detected in the peripheral blood of the elderly, and its expression level is elevated in patients with post-traumatic stress disorder [14]. Draxin expression is increased in the intestinal tissues of patients with inflammatory bowel disease and correlates with a poor response to treatment [15]. Furthermore, high draxin expression in gliomas correlates with a poor prognosis [16]. These findings suggest that draxin may exert a regulatory effect on the nervous system in adulthood and may have detrimental effects on mature neurons. Although direct evidence linking draxin to AD is limited, our previous bioinformatics analysis of the Alzheimer's disease database (AlzData) database

found that draxin expression in the hippocampus of AD patients is elevated compared with controls (p = 0.044). In addition, hydroxymethylation of the upstream region of the *draxindraxin* gene is associated with the formation of p-tau [17]. This suggests a potential role for draxin in the pathogenesis of AD, although the exact mechanism of action remains to be elucidated. In the present study, draxin was found to have injurious effects on mouse hippocampal neuronal cells. It was also found to increase the level of tau protein phosphorylation. Moreover, draxin overexpression significantly impaired the learning and memory capacities of mice and exacerbated the progression of AD-related pathology.

2. Materials and Methods

2.1 Mice, Brain Stereotactic Injection, and Experimental Groups

Male C57BL/6 mice (15 weeks old) weighing approximately 23–28 g were purchased from Jiangsu Jicui Pharmachem Biotechnology Co., Ltd. (Nanjing, Jiangsu, China). All mice were housed (five animals per cage) in specific pathogen-free facilities at the Guangdong Medical University Laboratory Animal Center. They were maintained at a constant temperature of 23 $\pm$ 2 °C, a relative humidity of 60 $\pm$ 5%, a 12-h light/12-h dark cycle, and with free access to food and water. Bedding and fresh water were replaced weekly, and every 5 days post-modeling. All animal-related experiments in this study were approved by the Ethics Committee of Guangdong Medical University (Ethics Approval No. GDMU-2023-000109) and adhered to international practices for animal experiments.

Phosphate-buffered saline (PBS), empty adeno-associated virus (AAV), and *draxin*-expressing AAV (GOSV0403972; Shanghai Genechem Co., Ltd., Shanghai, China) were delivered into the hippocampus of 15-week-old male C57BL/6 mice using stereotactic techniques. The animals were securely positioned in a stereotactic frame (018.116; NEUROSTAR, Malvern, PA, USA) with the head maintained in a flat skull position. The anterior fontanelle was exposed following a midline scalp incision with ophthalmic scissors. According to the mouse brain stereotactic atlas, the Cornu Ammonis 1 (CA1) region was targeted with the following coordinates relative to the anterior fontanelle: 2.1 mm posterior, 1.8 mm lateral from the midline, and 2.0 mm ventral from the skull surface. A total volume of 1 µL of each solution was slowly infused using a micro-syringe (980-02918-00; Ningbo Zhenhai Glass Instrument Factory, Ningbo, Zhejiang, China) at a rate of 0.1 µL/min. The needle was kept in place for an additional 5 min to facilitate adequate diffusion of the solution and minimize backflow. Subsequently, the needle was gradually withdrawn to prevent reflux. The wild-type C57BL/6 mice were assigned to three experimental groups based on the injected material. The wild-type (WT) +PBS group was injected with PBS, the WT+AAV-NC (negative control) group was injected with empty AAV, and the WT+AAV-draxin group was injected with *draxin*-expressing AAV. At the end of all experimental procedures (including behavioral tests), mice were euthanized via an intraperitoneal injection of sodium pentobarbital (150 mg/kg, Sigma-Aldrich, St. Louis, MO, USA) to ensure a humane death. Euthanasia was confirmed by the absence of vital signs (cessation of breathing, loss of corneal reflex, and no response to paw pinch) for at least 5 min. The brains were then rapidly dissected for subsequent histological and molecular analyses.

2.2 Cell Culture

The HT22 (iCell-m020) mouse hippocampal neuronal cell line used in the experiments was purchased from Cellverse (iCell) Bioscience Technology Co., Ltd. (Shanghai, China). All cells were authenticated by the vendor and tested negative for mycoplasma prior to use. Cell experiments were conducted in a sterile, ultra-clean facility within the cell room of the Institute of Neurology at Guangdong Medical University, adhering strictly to aseptic requirements. The cells were cultured in an incubator under optimal conditions, featuring a gas phase composition of 95% air and 5% carbon dioxide, a constant temperature of 37 °C, and a humidity range of 70%–80%.

2.3 Viruses Used for Overexpression

(1) Lentivirus: pHBLV-CMV-MCS-3FLAG-EF1-ZsGreen-T2A-PURO, an empty load virus, and a draxin-overexpressing virus were purchased from Hanheng Biotechnology Co., Ltd. (HH20221222GYQ-LV01, Shanghai, China).

(2) Adeno-associated virus: GV753-hsyn promoter-EGFP-FT2A-MCS-WPRE-SV40 PolyA, empty load virus, and draxin-overexpressing virus were purchased from GeneChem Co., Ltd. (GOSV0403972, Shanghai, China).

2.4 Cell Counting Kit-8 (CCK8) Assay

Cells with favorable viability were plated into 96-well plates for subsequent experiments, with cell numbers adjusted for the specific experimental requirements. For cell viability assays, approximately 2×10^3 cells were seeded per well, and the assay was performed after cells had fully adhered to the plate and reached an appropriate density. To determine the optimal Aβ42 (04010011526, Qiangyao Biotech Co., Ltd., Shanghai, China) concentration, around 1×10^4 cells were seeded into each well, followed by incubation with Aβ42 for 24 h before the assay. The CCK8 (CK04-11, DOJINDO Laboratories, Kyushu, Japan) assay was performed according to the manufacturer's instructions.

2.5 Protein Immunoblotting

Tissues were homogenized in lysis buffer (2500070007, Solarbio, Beijing, China) containing protease and phosphatase inhibitors (A32961; Thermo Fisher Scientific, MA, USA) and centrifuged at 12,000

rpm for 20 min at 4 °C. Supernatant was collected and the protein concentrations quantified using a bicinchoninic acid assay (BCA) (3213970, ThermoFisher Scientific, Waltham, MA, USA). Proteins (45 µg) were mixed with loading buffer, electrophoresed on SDS-PAGE gel, and then transferred to a polyvinylidene difluoride membrane (PVDF IPVH00010, Millipore Corporation, Burlington, MA, USA). The membranes were blocked with TBS/0.1% Tween-20 (TBST) buffer containing 5% bovine serum albumin (V900933-100G; Sigma-Aldrich) at room temperature, then incubated overnight at 4 °C with MAP2 antibody (rabbit, 1:1000, 8707S, Cell Signaling Technology, Danvers, MA, USA), NeuN antibody (rabbit, 1:1000, 24307S, Cell Signaling Technology), phosphorylated tau (Ser396) (p-tau396) antibody (rabbit, 1:1000, AB109390, Abcam, Cambridge, Cambridgeshire, UK), phosphorylated tau (Thr231) (mouse, 1:1000, PA5-117230, Invitrogen, MA, USA), draxin (sheep, 1:1000, CDUB03240, R&D Systems, Minneapolis, MN, USA), or primary antibodies to β-catenin (1:1000, 8480, Cell Signaling Technology), GSK-3β (1:1000, 9315S; Cell Signaling Technology), and lipoprotein receptor-related protein 6 (LRP6) (1:1000, 3395S; Cell Signaling Technology). All primary antibodies were obtained from Cell Signaling Technology. The membranes were then washed with TBST (five times for 3 min each) and incubated with secondary antibodies (1:10,000 in TBST, BA1054, Boster Biological Technology Co., Ltd., Wuhan, Hubei, China) for 1 h. Signals were visualized using enhanced chemiluminescence (ECL) (BMU102-CN, Abbkine Scientific Co., Ltd., Wuhan, Hubei, China) (Azure Biosystems C600, Dublin, CA, USA) and optical densities were analyzed using ImageJ software (v1.54f, National Institutes of Health, Bethesda, MD, USA). Specifically, quantification software and settings were as follows: the "Gels" tool of ImageJ v1.54f was used and band optical density (OD) was measured after background subtraction (rolling ball radius = 50 pixels). Additionally, normalization details were verified: loading control bands were confirmed to be within the linear range of detection via serial dilution validation, ensuring accurate normalization. For averaging of replicates, data from 3–4 independent biological replicates were first normalized to the loading control [vinculin (1:1000, 13901S; Cell Signaling Technology) or (glyceraldehyde-3-phosphate dehydrogenase) GAPDH (1:1000, 5174S; Cell Signaling Technology)] for each sample, then averaged to calculate the relative expression level [mean ± standard error of the mean (SEM)]. Furthermore, for western blot (WB) densitometry statistical analysis, one-way ANOVA (for multiple groups) or two-way ANOVA (for factorial designs) was used to compare relative expression levels, with Tukey's post-hoc test for pairwise comparisons (significance set at $p < 0.05$). Original Western blot images are provided in **Supplementary Material-WB Original**.

2.6 Quantitative Real-Time Polymerase Chain Reaction

Relative mRNA levels were measured via quantitative real-time polymerase chain reaction (qRT-PCR) with validated primer pairs (Table 1). Total RNA was extracted from cells using TRIzol reagent (15596018CN, Ambion, Austin, TX, USA) and cDNA was synthesized using a reverse transcription kit (RR820Q, TaKaRa, Shiga, Japan). The assays were performed on a LightCycler 96 quantitative PCR instrument (ABI QuantStudio 6 Pro, Thermo Fisher Scientific) and a 96-well optical plate [18].

Table 1. Primer sequences for qRT-PCR.

Gene name	Sequence
GAPDH-F	*TCCTGCACCACCAACTGCTTAG*
GAPDH-R	*TGCTTCACCACCTTCTTGATGTC*
Draxin-F	*CTGCTTCTGGGGCTGACTTTG*
Draxin-R	*CCTGCGTCTCTTGTGTTCTCTG*
IL-1β-F	*GGGCCTCAAAGGAAAGAATCT*
IL-1β-R	*GAGGTGCTGATGTACCAGTTGG*
IL-6-F	*TAGTCCTTCCTACCCCAATTTCC*
IL-6-R	*TTGGTCCTTAGCCACTCCTTC*
IL-10-F	*TGGTAGAAGTGATGCCCCAG*
IL-10-R	*ACTCTTCACCTGCTCCACTG*
TNF-α-F	*GTGGAACTGGCAGAAGAG*
TNF-α-R	*GAGAAGAGGCTGAGACATAG*

GAPDH, glyceraldehyde-3-phosphate dehydrogenase; Draxin, dorsal inhibitory axon guidance protein; IL, interleukin; TNF, tumor necrosis factor.

2.7 Tissue Immunofluorescence

Mouse brain sections were washed three times with PBS. They were blocked in PBS containing 10% normal goat serum (240528; Affinity Biosciences Ltd., Changzhou, Jiangsu, China) for 1 h at room temperature, then incubated overnight at 4 °C with the primary antibody. After washing with PBS, sections were incubated in blocking buffer with secondary antibodies for 1 h. Cell nuclei were stained with Hoechst 33342 (C0031-01, Solarbio) for 8 min at room temperature. Following three PBS washes, images were acquired using a confocal microscope (FV3000, Olympus, Tokyo, Japan). Primary antibodies used for immunostaining were MAP2 (rabbit; 1:200, Cell Signaling Technology) and NeuN (rabbit, 1:200, Cell Signaling Technology). Secondary antibodies were Alexa Fluor 488 streptavidin anti-biotin (1:400, 702410ES03, Yeasen Biotechnology, Shanghai, China) and Alexa Fluor 488/555 coupled goat anti-rabbit IgG (1:800, cr3358443-5, Abcam).

2.8 Water Maze Experiments

The Morris water maze (MWM) was used to evaluate spatial learning and memory in mice. Briefly, a circular pool (diameter 120 cm, height 50 cm) filled with water (22 ± 1 °C, water depth 30 cm) was rendered opaque with non-

toxic white pigment. A camera system was mounted vertically approximately 3 m above the pool. The pool was divided into four quadrants: east, west, south, and north, with a platform (diameter 12 cm, height 29 cm) placed centrally in the north quadrant. Distinctive visual cues (different colors/shapes) were fixed around the pool to aid platform localization. The 7-day test included three phases: visible platform training, hidden platform training, and probe trial (no platform). On day 1 (visible platform training), the platform was exposed 1 cm above the water, and each mouse was released into the water from the center of each quadrant (north, east, west, south). Latency to find the platform was recorded. Mice failing to locate the platform within 60 s were guided to the platform and allowed to stay for 15 s. A submerged platform (1 cm below the water) was used on days 2–6 (hidden platform training). Each mouse was trained four times per day and released from different quadrants in varying order. Escape latency (time to find the platform) was recorded, with training ending at the 60th second, and a 15-s temporary stay on the platform for mice failing to locate it. On day 7 (probe trial), the platform was removed. Spatial exploration was assessed by releasing mice from the quadrant opposite the original platform location. Data were analyzed by two-way repeated measures ANOVA.

2.9 Y-Maze Experiment

Spatial memory was assessed using a Y-maze with removable arm partition baffles, as previously described [19]. Mice were habituated to the experimental environment for 1 week before the formal experiment. After habituation, distinct colored and shaped stickers were affixed to the end of each arm. The formal experiments commenced with each mouse tested for 10 min per session. The Y-maze experiment consisted of two phases, spaced 1 h apart. During the first phase of training, the novel arm was blocked with a partition baffle, and mice were placed at the end of the starting arm. After 10 min of free exploration at the starting arm and other accessible arms, mice were returned to their home cages. The second phase of the test was conducted 1 h later, with the partition baffle removed from the novel arm, and each mouse repositioned at the end of the starting arm. The time spent, distance traveled, and number of arm entries were recorded during 10 min of free exploration across all three arms.

2.10 AD Database Mining and Analysis

Draxin expression data were acquired from the AD-dedicated database AlzData (http://www.alzdata.org/) by integrating five publicly available gene expression datasets (GSE28146, GSE29378, GSE36980, GSE48350, GSE5281). Samples were selected based on three stringent criteria: human hippocampal tissue, clear grouping into AD patients or age-matched normal controls, and $\geq$90% data integrity. The final cohort comprised 68 AD and 52 normal controls, with all AD cases conforming to the National Institute on Aging and Alzheimer's Association (NIA-AA) diagnostic criteria. Dataset-specific sample sizes were as follows: GSE28146 (AD n = 12, control n = 8), GSE29378 (AD n = 15, control n = 10), GSE36980 (AD n = 14, control n = 9), GSE48350 (AD n = 13, control n = 12), and GSE5281 (AD n = 14, control n = 13). Data analysis was performed using R software (v4.3.0, R Core Team, Vienna, Austria). Quantile normalization was applied to eliminate inter-dataset batch effects. The limma package (3.54.1, Gordon K. Smyth, Walter and Eliza Hall Institute of Medical Research, Melbourne, VIC, Australia) was used for linear model fitting to calculate draxin's Log2 fold change (Log2FC) between the AD and control groups, two-tailed *t*-tests generated raw *p*-values, and the Benjamini-Hochberg method was employed to adjust for false discovery rate (FDR), with significance thresholds set at $p < 0.05$ and FDR <0.2. To ensure the robustness and reliability of the integrated analysis, we performed additional reproducibility and sensitivity checks. Reproducibility check: we re-analyzed each dataset independently (rather than only integrating them) and confirmed consistent upregulation of draxin in AD hippocampi across all five datasets ($p < 0.05$ for GSE28146, GSE29378, and GSE5281; $p < 0.1$ for GSE36980 and GSE48350), supporting the robustness of the finding. Sensitivity analysis: exclusion of any single dataset did not alter the overall result (pooled $p < 0.05$), indicating the integrated analysis was not biased by individual datasets.

2.11 Data Analysis

Images were analyzed using ImageJ. All data were expressed as the mean $\pm$ SEM and analyzed using one-way ANOVA or two-way ANOVA for multiple comparisons. The significance level was set at $p < 0.05$. The statistical software used in the study was GraphPad Prism 9.0 (GraphPad Software, Inc., San Diego, CA, USA) for Windows.

3. Results

3.1 Elevated Draxin Expression in the Hippocampus of AD Patients, and Construction of Draxin-Overexpressing Mouse and AD Cell Models

Following a search of the AD database AlzData—encompassing the publicly available datasets GSE28146, GSE29378, GSE36980, GSE48350, and GSE5281—draxin expression in the hippocampal region of AD patients was found to be higher than in normal subjects ($p = 0.044$; Fig. 1A). After considering data from multiple brain regions, no difference in the FDR was found (Fig. 1B). To investigate the role of draxin overexpression in the pathogenesis and progression of AD, we constructed a mouse model of draxin overexpression by injecting *draxin*-AAV into the bilateral hippocampus of WT mice. The spontaneous green fluorescent protein (GFP) green signal of the virus was visualized using fluorescence microscopy (Fig. 1C). A qRT-PCRassay showed that the level of draxin expression in

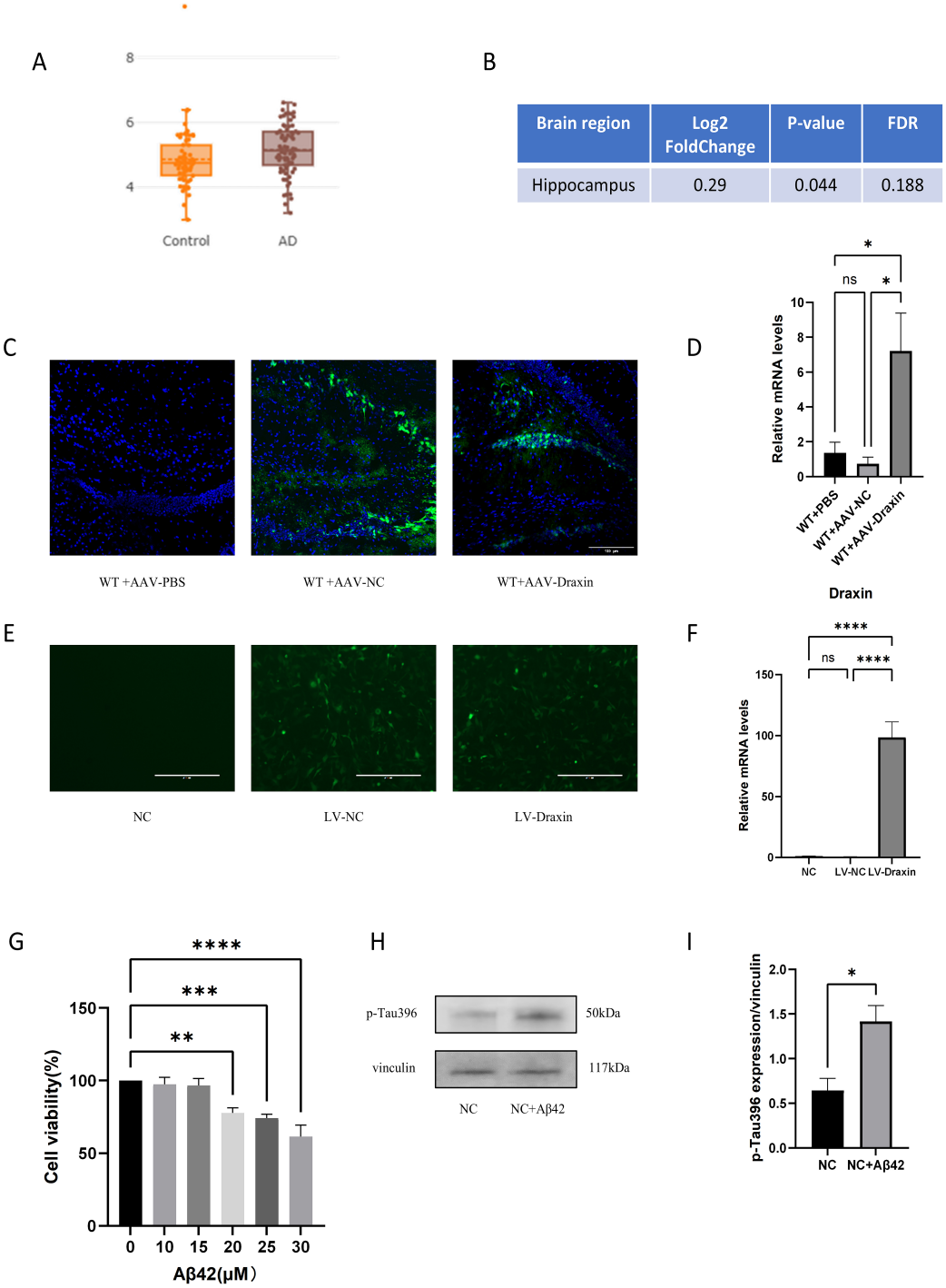

Brain region	Log2 FoldChange	P-value	FDR
Hippocampus	0.29	0.044	0.188

Fig. 1. Expression of draxin in the hippocampus of AD patients in AlzData. (A) Distribution of draxin expression in the hippocampus of AD patients and normal subjects (n = 68 in control group, n = 52 in AD group); (B) Draxin expression in the hippocampus of AD patients and normal subjects. (C) Fluorescence microscopy of the hippocampal gland of three groups of mice with different virus expression. Scale bar = 100 μm. (D) qRT-PCR detection of hippocampal draxin expression in three groups of mice. n = 4. * $p < 0.05$; ns, $p > 0.05$. (E) Fluorescence microscopy of draxin lentivirus after transfection of HT22 cells. Scale bar = 100 μm. (F) *Draxin* mRNA expression in cells from the three groups. n = 4. **** $p < 0.0001$ for LV-draxin compared with the NC and LV-NC groups; ns for NC compared with the LV-NC control group, $p > 0.05$. (G) Changes in cell viability after treatment of HT22 cells with different concentrations of Aβ42; **** $p < 0.0001$; *** $p < 0.001$; ** $p < 0.01$. (H) Western blot detection of changes in the expression of p-Tau396 after treatment of HT22 cells with an Aβ42 concentration of 20 μM, n = 4; (I) Quantification of changes in the expression of p-Tau396. n = 3. mean ± SEM, * $p < 0.05$. AD, Alzheimer's disease; FDR, false discovery rate; WT, wild-type; AAV, adeno-associated virus; PBS, phosphate-buffered saline; NC, negative control; LV-NC, lentivirus-negative control; Aβ42, amyloid-β-42; p-Tau, phosphorylated tau protein.

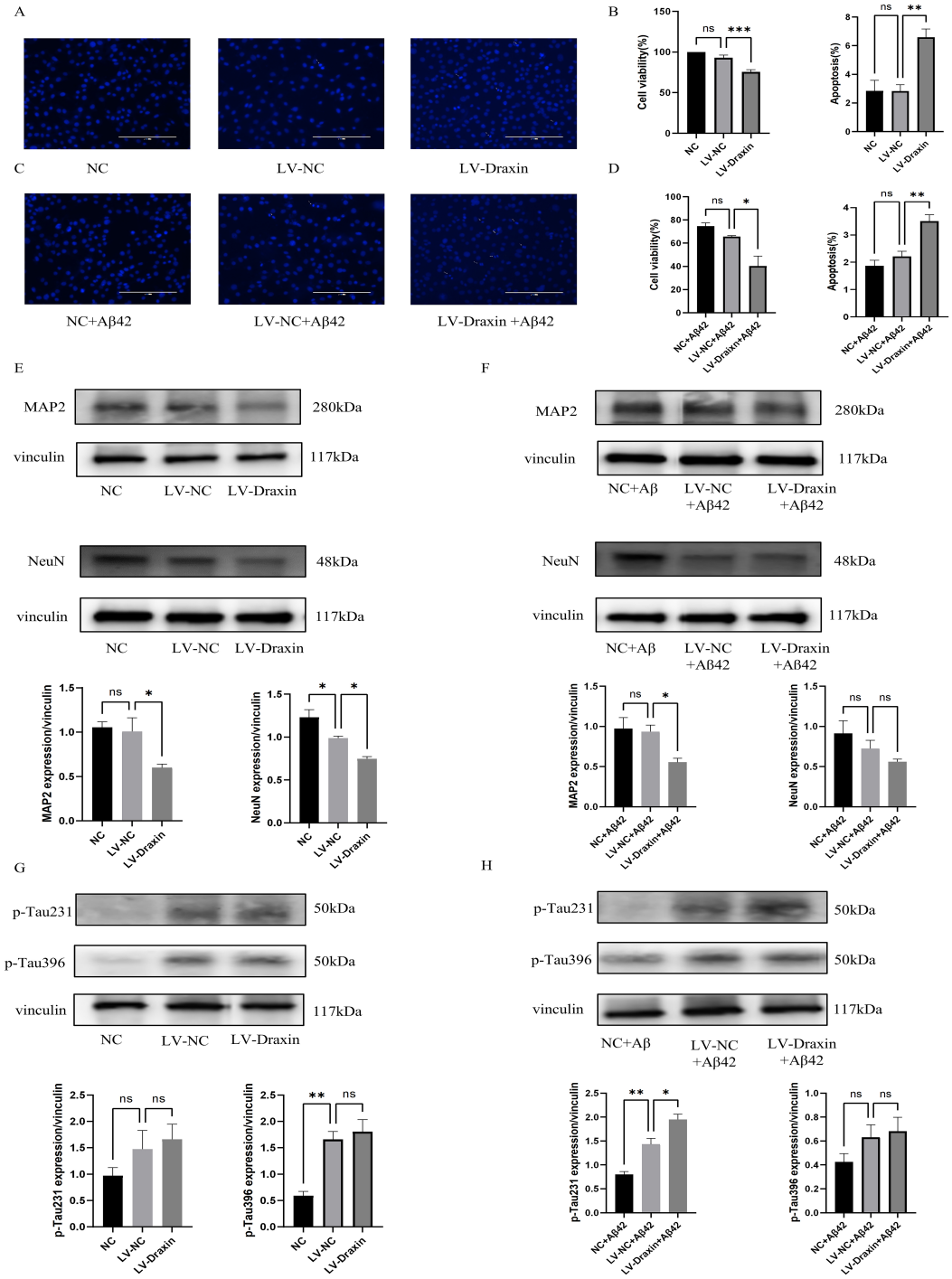

Fig. 2. Effects of draxin on the activity, neuronal-associated proteins, and Tau proteins of HT22 cells and AD cell models. (A) Hoechst staining of the three groups of cells. Scale bar = 200 μm; (B) Cell survival rate, as determined by CCK8 assay. Hoechst staining of the three groups of cells was used to calculate the apoptosis rate. (C) Hoechst staining of three AD cell models. Scale bar = 200 μm; (D) Cell viability, as determined by CCK8 assay, and apoptosis rate as determined by Hoechst staining of the three AD cell models. (E) Western blot detection of MAP2 and NeuN expression, and quantification of the results in three groups of HT22 cells, MAP2 n = 3, NeuN n = 4. (F) Western blot detection of MAP2 and NeuN expression, and quantification of the results in three groups of AD cell models, MAP2 n = 3, NeuN n = 3. (G) Western blot detection of p-Tau231 and p-Tau396 expression and quantification of the results in three groups of HT22 cells, p-Tau231 n = 4, p-Tau396 n = 4; (H) Western blot detection of p-Tau231 and p-Tau396 expression and quantification of the results in three groups of AD cell models, p-Tau231 n = 4, p-Tau396 n = 4. mean ± SEM, *** $p < 0.001$; ** $p < 0.01$, * $p < 0.05$, ns, $p > 0.05$. Aβ, amyloid-β; CCK8, Cell Counting Kit-8; MAP2, microtubule-associated protein 2; NeuN, neuronal nuclear antigen.

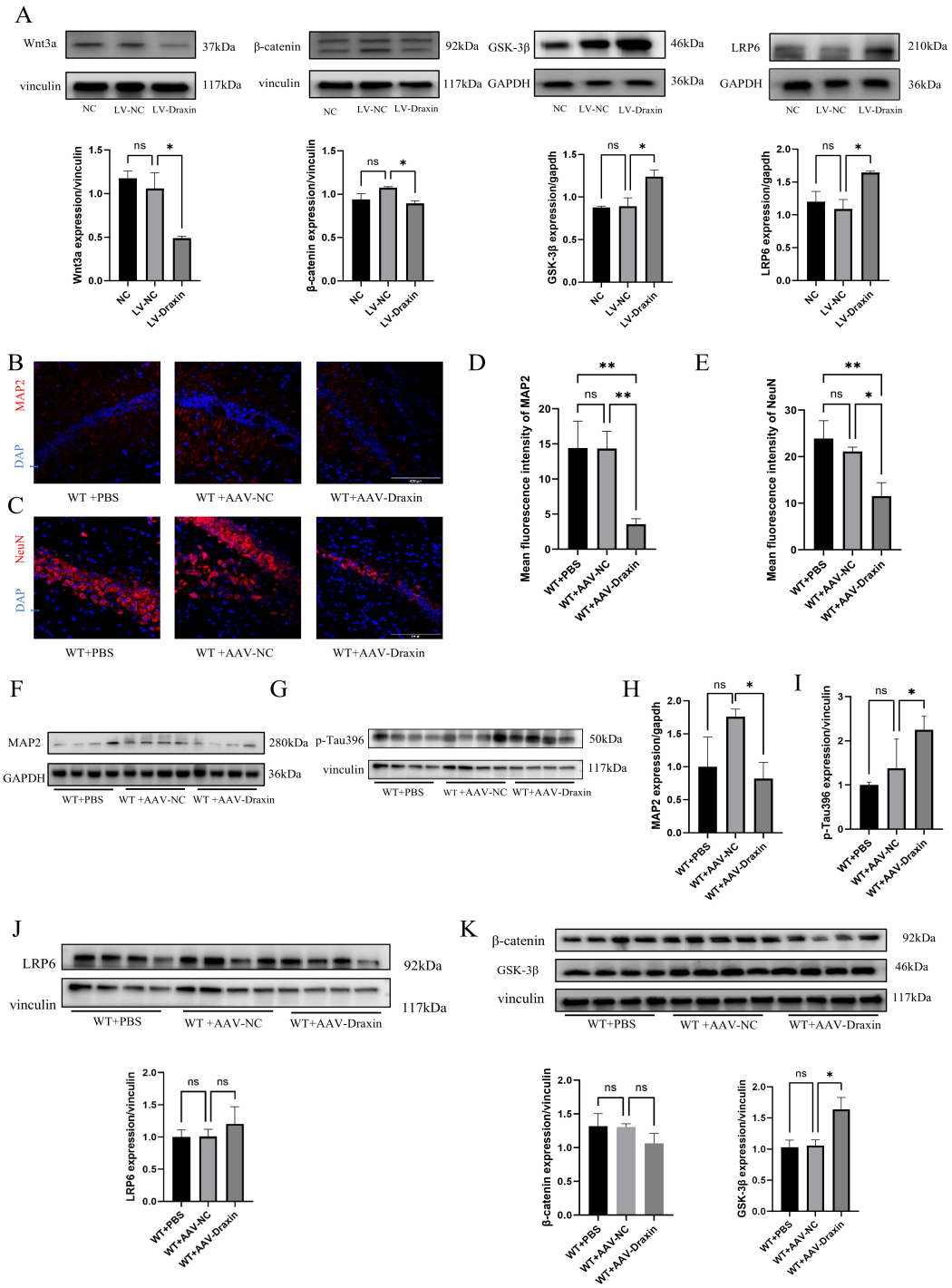

Fig. 3. The effect of draxin on the levels of Wnt/β-catenin/GSK-3β pathway-related proteins in HT22 cells and normal mouse hippocampus, as well as the expression of normal hippocampal neuron-related proteins and Tau protein phosphorylation levels. (A) Western blot detection of Wnt3a, β-catenin, GSK-3β, and LRP6 expression in three groups of cells, and quantification of the results, Wnt3a n = 3, β-catenin n = 4, GSK-3β n = 3, LRP6 n = 3. (B,D,F,H) Immunofluorescence and Western blot detection of hippocampal MAP2 expression in three groups of mice, and quantification of the results, n = 4. (B,C): scale bar = 400 μm) (D,E,G,H,I) Immunofluorescence and Western blot detection of hippocampal NeuN expression in three groups of mice, and quantification of the results, n = 4; (J) Changes in the expression of LRP6 in three groups of mice, and quantification of the results, n = 4; (K) Western blot detection of Wnt/β-catenin/GSK-3β pathway-related protein expression in three groups of mice, and quantification of the results, n = 4. mean ± SEM, * $p < 0.05$; ** $p < 0.01$; ns, $p > 0.05$. GSK-3β, glycogen synthase kinase-3β; LRP6, lipoprotein receptor-related protein 6.

the WT+AAV-draxin group was significantly increased relative to the WT+PBS and WT+AAV-NC groups ($p < 0.05$; Fig. 1D).

An AD cell model with overexpression of draxin was also constructed with HT22 cells. After mapping the optimal Multiplicity of Infection (MOI), draxin lentivirus was successfully transfected into HT22 cells, with the spontaneous GFP green signal of the virus visible by fluorescence microscopy (Fig. 1E). qRT-PCR revealed that draxin expression was significantly higher in the lentivirus (LV)-draxin group compared with the negative control (NC) and lentivirus-negative control (LV-NC) groups ($p < 0.0001$; Fig. 1F), indicating successful construction of the HT22 cell model with draxin overexpression. To select the optimal Aβ concentration, HT22 cells were treated with Aβ42 (0–50 µM) for 24 h, and their viability was then quantified using a CCK8 assay. A dose-dependent reduction in viability ($p < 0.05$ vs control) was observed starting at 20 µM ($p < 0.01$; Fig. 1G). After the treatment of cells with Aβ42 at a concentration of 20 µM, western blotting showed significantly increased tau protein phosphorylation ($p < 0.05$; Fig. 1H,I). Therefore, a 20 µM concentration was selected to treat HT22 cells and AD cell model constructs.

3.2 Draxin Overexpression Reduces Cell Viability and the Expression of Neuronal Marker Proteins MAP2 and NeuN in HT22 Cells and AD Cell Models

To investigate whether draxin has a detrimental impact on hippocampal neuronal cells, the viability of cells in the NC, LV-NC, and LV-draxin groups was evaluated by CCK8 assay, while the apoptosis rate was assessed by Hoechst staining. The survival rate of cells in the LV-draxin group was significantly decreased compared with the LV-NC group ($p < 0.001$; Fig. 2A), while the apoptosis rate was significantly increased ($p < 0.01$; Fig. 2B). Similar results were observed in the AD cell model constructed with HT22 cells and Aβ42, with the survival rate of cells in the LV-draxin+Aβ42 group being significantly decreased, while the apoptosis rate was significantly increased ($p < 0.05$; Fig. 2C,D). The expression levels of MAP2 and NeuN are shown in Fig. 2E. The expression of MAP2 and NeuN was lower in the LV-draxin group compared with the LV-NC+Aβ42 group, reaching significance for MAP2 ($p < 0.05$; Fig. 2F).

3.3 Effects of Draxin Over-Expression on Tau Protein Phosphorylation and the Expression of Wnt/β-Catenin/GSK-3β Pathway Components in HT22 Cells and AD Cell Models

To determine whether draxin aggravated AD pathology, we examined the expression levels of p-tau in three groups of cells: NC, LV-NC, and LV-draxin. A trend for increased levels of phosphorylated tau proteins p-tau231 and p-tau396 was observed in the LV-draxin group in contrast to the LV-NC group (Fig. 2G). The level of phosphorylated tau protein p-tau396 in the NC group was significantly higher than in the LV-NC group ($p < 0.01$), while p-tau231 showed a non-significant increase ($p > 0.05$). The expression level of tau proteins in NC+Aβ42, LV-NC+Aβ42, and LV-draxin+Aβ42 cells is shown in Fig. 2H. The expression of p-tau231 was significantly increased in the LV-draxin+Aβ42 group compared with the LV-NC+Aβ42 group ($p < 0.05$), while the expression of p-tau396 showed a non-significant increase ($p > 0.05$). In the LV-NC+Aβ42 group, the expression of p-tau231 was significantly increased ($p < 0.01$), while p-tau396 showed a non-significant increase ($p > 0.05$) compared with the NC+Aβ42 group. Subsequently, we also evaluated the expression level of Wnt/β-catenin/GSK-3β pathway components (Fig. 3A). The expression of Wnt3a and β-catenin was significantly downregulated in the LV-draxin group compared with the LV-NC group ($p < 0.05$), while GSK-3β and LRP6 expression was upregulated ($p < 0.05$). The LV-NC group showed no significant differences in the expression of Wnt3a, β-catenin, GSK-3β, and LRP6 compared with the NC group (all $p > 0.05$). Collectively, these findings suggest that overexpression of draxin in HT22 cells promotes the phosphorylation of tau proteins through activation of the Wnt/β-catenin/GSK-3β pathway, especially when stimulated by Aβ42.

3.4 Draxin Overexpression Impairs Spatial Learning and Memory Ability in Mice

The Y-maze test and MWM were used to evaluate the learning and memory ability in the three groups of mice: WT+PBS, WT+AAV-NC, and WT+AAV-draxin. The spontaneous alternation rate (alternation %) of mice in the WT+AAV-draxin group was significantly lower than in the WT+AAV-NC group ($p < 0.01$; Fig. 4A,B). The spatial recognition experiments revealed no significant differences between the three groups in terms of the number of new arm entries (number of new arms) and the percentage of exploration time in the new arm (time in the new arm%) ($p > 0.05$; Fig. 4B).

In the MWM experiments, the time to find the platform (platform latency) of the mice decreased progressively over time during navigation training in the WT+AAV-NC and WT+PBS groups, but not in the WT+AAV-draxin group (Fig. 4C,D). In the probe experiment on day 6, mice in the WT+AAV-draxin group exhibited a significantly decreased number of platform crossings compared with the other two groups ($p < 0.001$), as well as decreased time and distance in the target quadrant ($p < 0.05$; Fig. 4E). These results suggest that draxin overexpression in the mouse brain leads to a decline in spatial learning and memory ability.

3.5 Neuropathological Changes in WT Mice Induced by Draxin Overexpression

Neuropathological changes in the mouse brain were examined by detecting the expression of MAP2, NeuN, and p-tau, as well as the Wnt/β-catenin/GSK-3β pathway

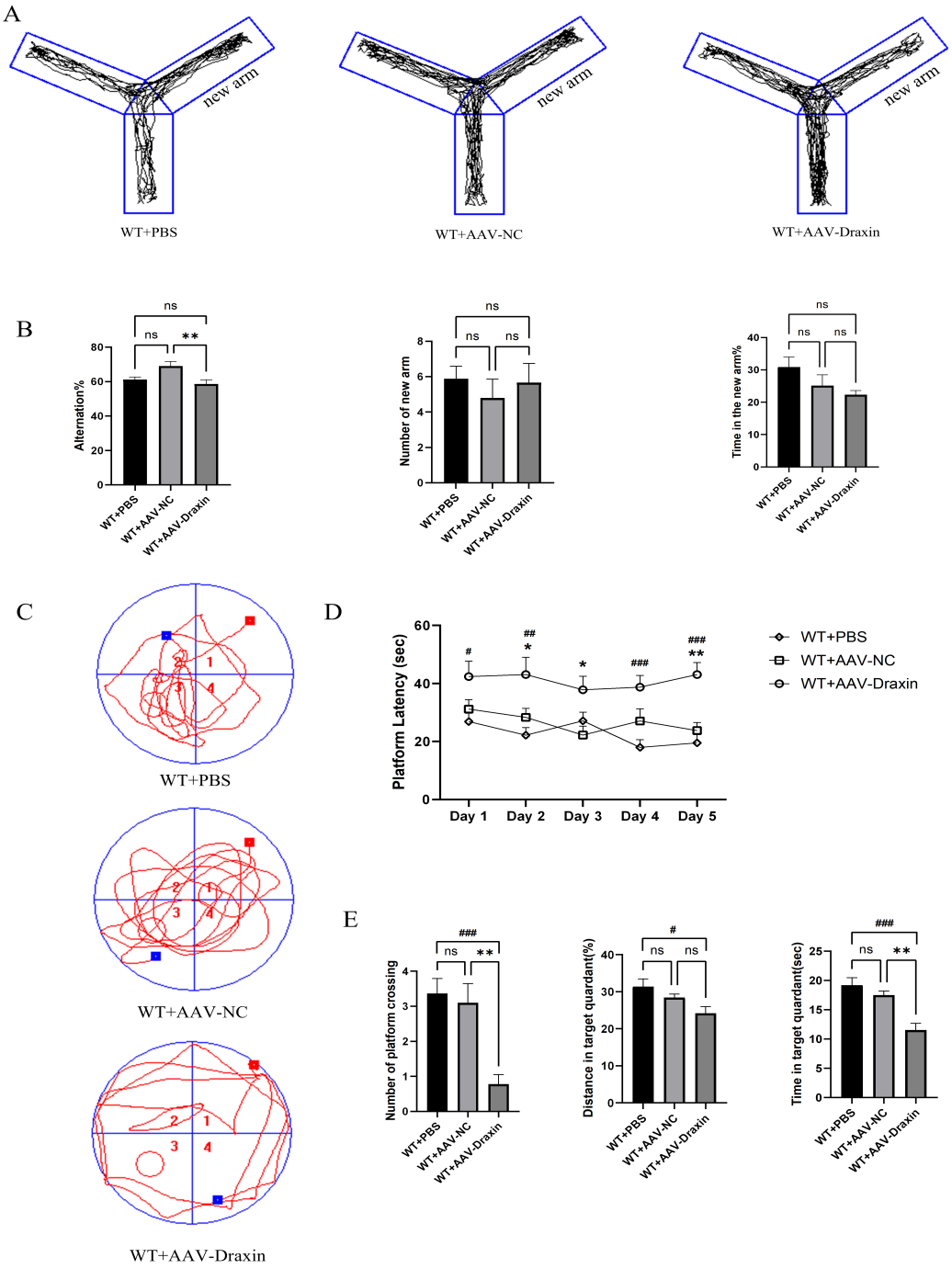

Fig. 4. Behavioral experiments aimed at detecting the effects of draxin on the learning and memory ability of normal mice. (A) Motion trajectory diagrams of mice from the three groups exploring the new arm of the Y maze spatial recognition experiment. (B) Y maze spontaneous alternation rate, number of times exploring the new arm, and percentage of time exploring the new arm by the three groups of mice in the alternation experiment; n = 10. ** $p < 0.01$; ns, $p > 0.05$. (C) Typical movement trajectory diagrams of the spatial exploration phase of the three groups of mice; Red dots = Mice starting points; Blue dots = Mice end points; (D) Time required to find the platform in the localization and navigation experiments of the three groups of mice (evasion latency); (E) Number of times traversing the platform in the spatial exploration phase, percentage of swimming distance in the quadrant where the platform was located during the exploration phase, and percentage of time spent on the platform in the spatial exploration phase of the three groups of mice. Percentage of swimming distance in the quadrant where the platform was located, and the time spent in the exploration phase where the platform was located; n = 10. * $p < 0.05$, ** $p < 0.01$ compared to the WT+AAV-NC group; ns, $p > 0.05$; $^{\#}$ $p < 0.05$, $^{\#\#}$ $p < 0.01$, $^{\#\#\#}$ $p < 0.001$ compared to the WT+PBS group; ns, $p > 0.05$.

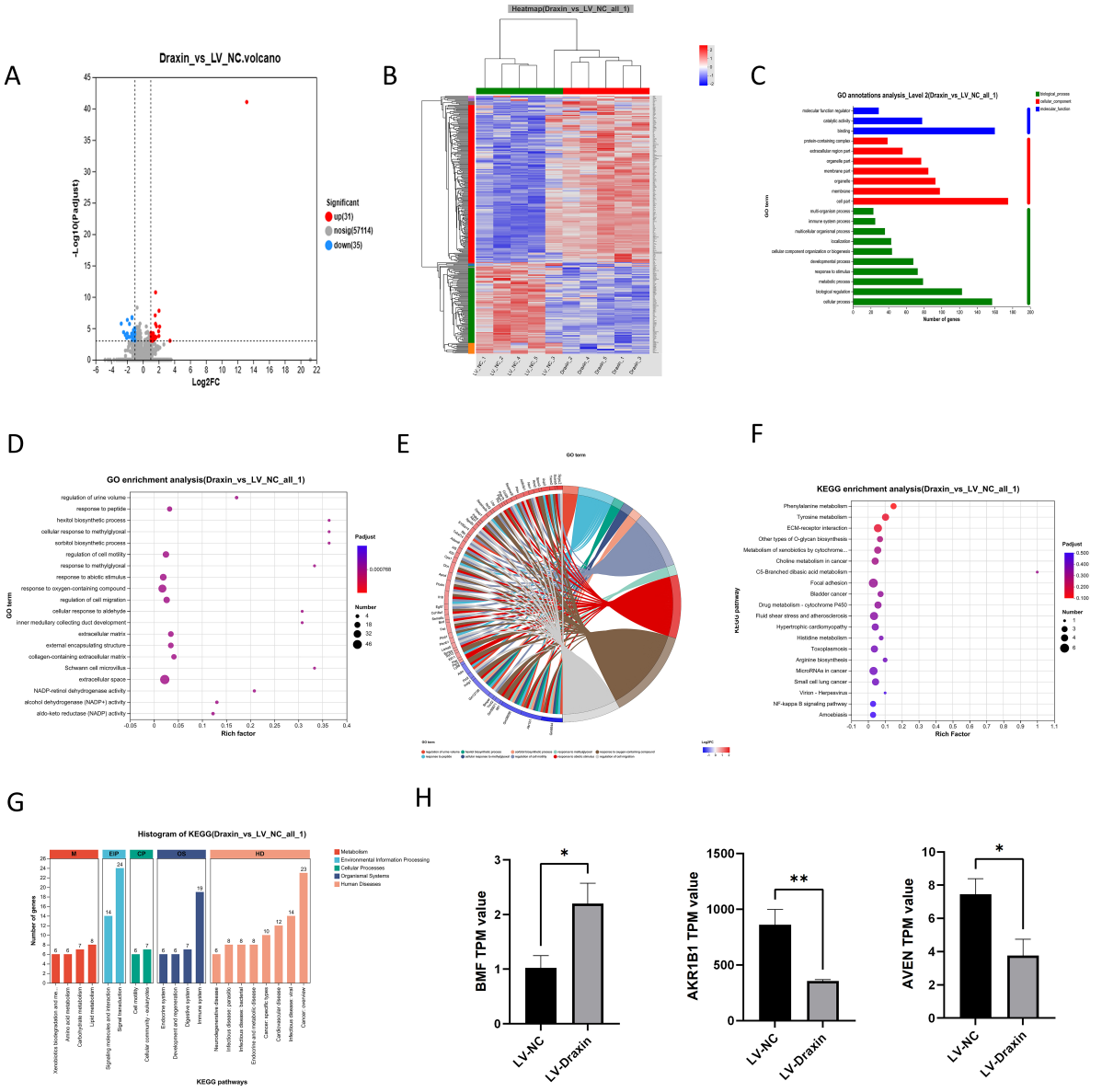

Fig. 5. RNA sequencing analysis of HT22 cells with draxin overexpression. (A) Differential gene volcano plot; (B) Clustering heatmap of differentially expressed genes (red color indicates up-regulated gene expression; blue color indicates down-regulated gene expression); (C) Differentially expressed gene GO function annotation map; (D) Differentially expressed gene GO enrichment bubble map; (E) Differentially expressed gene GO enrichment string map; (F) Differentially expressed gene KEGG function annotation map; (G) Differentially expressed gene KEGG enrichment bubble map; (H) Relative expression of *BMF*, *AKR1B1* and *AVEN* genes in the cells of the two groups. n = 5. * $p < 0.05$; ** $p < 0.01$. GO, Gene Ontology; KEGG, Kyoto Encyclopedia of Genes and Genomes; BMF, BCL2-modifying factor; AKR1B1, Aldo-keto reductase family 1 member B1.

(Fig. 3). Immunofluorescence (IF) revealed significantly decreased expression of MAP2 and NeuN in the WT+AAV-draxin group compared with the WT+AAV-NC group ($p < 0.05$; Fig. 3B–E). Western blot results showed that MAP2 expression in the hippocampus of mice from the WT+AAV-draxin group was significantly decreased compared with the WT+AAV-NC group (Fig. 3F,H). There was no significant difference in the expression levels of MAP2 and NeuN between the WT+AAV-NC and WT+PBS groups.

The level of p-tau396 in mice from the WT+AAV-draxin group was increased compared with the WT+AAV-NC group ($p < 0.01$; Fig. 3G,I–K), while no significant difference was observed between the other two groups (Fig. 3G,I). GSK-3β expression was also increased in the WT+AAV-draxin group ($p < 0.05$), while β-catenin showed a non-significant decrease, and LRP6 a non-significant increase ($p > 0.05$). These results suggest that draxin overexpression in the mouse hippocampus promotes

pathological hyperphosphorylation of tau protein, as well as neuronal damage that appears to be mediated by the Wnt/β-catenin/GSK-3β pathway.

3.6 Transcriptomic Sequencing of HT22 Cells With Draxin Overexpression

To explore the mechanisms underlying the detrimental impacts of draxin overexpression on the brain and neurons, RNA sequencing analysis was performed on HT22 cells from the LV-NC and LV-draxin groups. Significant changes were found in the expression of 66 genes, of which 31 were up-regulated and 35 were down-regulated (Fig. 5A). Heatmap clustering analysis showed different expression patterns among the samples (Fig. 5B). Gene ontology (GO) and kyoto encyclopedia of genes and genomes (KEGG) analyses revealed that the top 20 differentially expressed genes were significantly enriched in pathways for regulation of ribonuclease activity, adhesion of symbiont to host, response to protozoan, cellular response to interferon-beta, defense response to symbiont, defense response to virus, and regulation of nuclease activity. Amongst these, binding, cell part, and cellular process-related genes accounted for the highest percentage of biological processes (BP), cellular components (CC), and molecular functions (MF) (Fig. 5C).

Further analysis showed that draxin overexpression had a significant effect on hippocampal neuron glucose metabolism and alcohol metabolism, as well as regulating the stress response of aldehydes and the microvillus function of Schwann cells (Fig. 5D,E). KEGG enrichment analysis revealed that the differentially expressed genes were involved in a variety of metabolic regulations, with C5-branched-chain dicarboxylic acid metabolism (rich factor close to 1) being particularly significant. These genes were also enriched for biological processes such as the NF-κB signaling pathway and extracellular matrix (ECM)-receptor interactions, and were associated with a variety of human diseases (Fig. 5F). Pathway analysis further revealed the important roles of the differentially expressed genes in glucose metabolism, lipid metabolism, amino acid metabolism, signaling, and the immune system (Fig. 5G). Finally, expression of the pro-apoptotic gene BCL2-modifying factor (BMF) was significantly elevated in the LV-draxin group ($p < 0.05$), whereas expression of the anti-apoptotic genes aldo-keto reductase family 1 member B1 (AKR1B1) ($p < 0.01$) and apoptosis and caspase activation inhibitor (AVEN) ($p < 0.05$) were significantly reduced (Fig. 5H), suggesting that draxin may affect cell fate by regulating apoptosis-related genes.

4. Discussion

Elevated draxin expression in the hippocampus of AD patients has not been previously documented. The current study revealed for the first time the effects of draxin overexpression on mouse neurons and cognitive functions. This encompasses decreased expression of neuronal markers (MAP2, NeuN) and deficits in spatial learning and memory. Furthermore, draxin overexpression significantly promoted tau protein phosphorylation (p-tau231 and p-tau396) and neuronal apoptosis and inhibited the Wnt/β-catenin signaling pathway by activating GSK-3β. Collectively, these results imply a plausible pathogenic role of draxin overexpression in AD development and progression.

MAP2 is considered a useful marker for mature neuronal cells. NeuN, a protein encoded by the *RBFOX3* gene, is also commonly used as a neuronal biomarker. Previous studies have reported that draxin inhibits neuronal axon growth *in vitro* [20,21] and *in vivo* [22,23]. This is consistent with the present findings that draxin decreased cell viability, decreased the expression of MAP2 and NeuN, and increased the apoptosis rate in HT22 cells and an Aβ42-induced HT-22 AD-like cellular model. Tau protein critically maintains the stability of microtubules by orchestrating their structural organization in neurons. Abnormally elevated levels of p-tau, such as phosphorylated tau threonine 231 (p-tau231) and serine 396 (p-tau396), constitute the pathological basis for neurofibrillary tangle formation (NTF), which represents a hallmark pathological feature of AD [23,24]. Draxin overexpression gave rise to marked elevation of p-tau396 in HT22 cells, and p-tau231 in the Aβ42-induced HT-22 AD-like cellular model. These phosphorylation sites (p-tau231 and p-tau396) cooperatively promote NTF, with p-tau231 emerging earlier in AD progression than p-tau396 [25]. Our findings suggest that draxin overexpression causes direct neuronal injury and subsequent pathological changes.

Furthermore, draxin overexpression in WT mice resulted in spatial learning and memory dysfunction, as indicated by decreased time spent exploring the new arm in the Y-maze, prolonged escape latency, and reduced platform crossings in the MWM test. Moreover, mice with draxin overexpression showed reduced levels of hippocampal MAP2 and NeuN expression, along with elevated p-tau396. Draxin has been reported to be a competitive antagonist of Wnt proteins for binding to low-density LRP6, which in turn inhibits the classical Wnt/β-catenin signaling pathway [26]. The Wnt/β-catenin/GSK-3β pathway plays a pivotal role in neurogenesis, synaptic plasticity, and neuronal migration and differentiation, all of which are dysregulated in AD. Consequently, we systematically analyzed the expression profiles of key components in this signaling pathway. Decreased Wnt3a and β-catenin expression, and increased GSK-3β and LRP6 expression were found in the LV-draxin group, suggesting that draxin overexpression causes disruption of the Wnt3a/β-catenin/GSK-3β pathway.

GSK-3β is a key enzyme in tau protein hyperphosphorylation. Immunohistochemical analysis has revealed that GSK-3β activity in the cerebral cortex of AD patients is significantly higher than in healthy controls, and co-localized with Aβ plaques and neurofibrillary tangles [27]. GSK-3β

exacerbates neuronal dysfunction by phosphorylating tau and destabilizing microtubules. Additionally, it indirectly impairs the neuroprotective effects of the Wnt/β-catenin pathway by suppressing β-catenin stability [28,29]. The observed increase in p-tau elicited by draxin overexpression could potentially result from inhibitory effects on the Wnt3a/β-catenin/GSK-3β signaling pathway. This suggests that draxin may broadly affect signaling, metabolic regulation, organelle function, the cytoskeleton, the stress response, and the growth and differentiation of hippocampal neurons.

RNA sequence analysis revealed that relative expression of the *BMF* gene was significantly higher in the LV-draxin group compared with the LV-NC group, whereas the relative expression of *AKR1B1* (aldo-keto reductase family 1 member B1) and *AVEN* (apoptosis and caspase activation inhibitor) was significantly lower. BMF is a member of the B-cell lymphoma-2 (Bcl-2) family of proteins, and promotes or inhibits cell death by regulating the mitochondrial pathway [30]. BMF protein regulates the permeability of the mitochondrial membrane by binding to other Bcl-2 family proteins, promoting destabilization of the mitochondrial membrane and the release of apoptosis-associated proteins [31]. Increased expression of BMF is usually associated with activation of the apoptotic pathway [31]. The *AKR1B1* gene encodes a key enzyme that is involved in a variety of biological processes, including antioxidant defense [32] and metabolic homeostasis [33]. The downregulation of AKR1B1 in neurons may reduce cellular resistance to oxidative stress and increase the risk of cellular damage, thereby promoting apoptotic pathways. AVEN is known to inhibit apoptosis, in particular by interacting with Apaf-1, which blocks the release of cytochrome c from mitochondria to the apoptotic signaling pathway in the cytoplasm [34]. Thus, downregulation of AVEN may render neurons more susceptible to undergoing programmed cell death. Both the upregulation of BMF and the downregulation of AKR1B1 and AVEN suggest that draxin overexpression could potentially modulate AKR1B1- and AVEN-mediated apoptosis-related signaling pathways, although this requires further research.

In summary, our study demonstrated that draxin overexpression impairs learning and memory abilities in mice. This appears to be mediated by inhibition of the Wnt/β-catenin/GSK-3β signaling pathway, resulting in elevated tau phosphorylation and neuronal injury. Further studies are needed to fully elucidate the molecular mechanisms involving draxin in AD.

5. Conclusions

Our research yields strong evidence indicating that overexpressed draxin leads to cognitive dysfunction in mice through its damaging effects on hippocampal neurons. Suppression of the Wnt/β-catenin/GSK-3β signaling pathway may represent a potential underlying mechanism.

Abbreviations

AD, Alzheimer's disease; NFTs, neuroprogenitor fibrillary tangles; DCX, doublecortin; Sox2, sex determining region Y-box 2; PBS, phosphate-buffered saline; AAV, adeno-associated virus; CA1, Cornu Ammonis 1; qRT-PCR, quantitative real-time polymerase chain reaction; MWM, Morris Water Maze; FDR, false discovery rate; WT, wild-type; NC, negative control; BMF, BCL2-modifying factor; AVEN, Apoptosis And Caspase Activation Inhibitor; AKR1B1, Aldo-keto reductase family 1 member B1.

Availability of Data and Materials

The data presented in this study are available from the corresponding author upon request.

Author Contributions

ZL designed the study, directed the project, supervised the experiments and analyses, reviewed the manuscript, QC and YF performed experiments, interpreted results, and wrote the initial manuscript; LH participated in the acquisition of experimental data (Tissue Immunofluorescence) and the interpretation of key experimental data, drafted sections of the manuscript, and critically reviewed and edited the manuscript for important intellectual content. XC participated in the study design, provided targeted supervision on experimental design optimization, offered substantive intellectual input in the interpretation of complex data sets (RNA sequencing analysis), and participated in drafting and revising the initial manuscript. All authors contributed to editorial changes in the manuscript. All authors read and approved the final manuscript. All authors have participated sufficiently in the work and agreed to be accountable for all aspects of the work.

Ethics Approval and Consent to Participate

All animal-related experiments in this study were approved by the Ethics Committee of Guangdong Medical University (Ethics Approval No. GDMU-2023-000109) and adhered to the National Institutes of Health Guide for the Care and Use of Laboratory Animals (NIH Guide), a widely recognized international standard for the ethical care and use of laboratory animals.

Acknowledgment

Not applicable.

Funding

This research was funded by Guangdong Provincial Basic and Applied Basic Research Fund (2024A1515220002), the Clinical + Basic Research Project of Guangdong Medical University (4SG23284G, GDMULCJC2024003, GDMULCJC2024036), the Affiliated Hospital of Guangdong Medical University

(LCYJ2020B009), the Guangdong Provincial Medical Association Clinical Research Fund - Healthcare Special (2024HY-A6006), the 2023 Special Project of the Songshan Lake Medical-Engineering Integration Innovation Center of Guangdong Medical University (4SG22307P), the Guangdong Medical University Affiliated Hospital High level Talent Research Launch Fund (GCC2022011), the Science and Technology Planning Project of Zhanjiang (2020B01395, 2020B01421), the Science and Technology Planning Project of GDMU (GDMUQ2021047, GDMU2021122).

Conflict of Interest

The authors declare no conflict of interest.

Supplementary Material

Supplementary material associated with this article can be found, in the online version, at https://doi.org/10.31083/JIN47749.

References

[1] Winblad B, Amouyel P, Andrieu S, Ballard C, Brayne C, Brodaty H, *et al*. Defeating Alzheimer's disease and other dementias: a priority for European science and society. The Lancet. Neurology. 2016; 15: 455–532. https://doi.org/10.1016/S1474-4422(16)00062-4.

[2] Spalding KL, Bergmann O, Alkass K, Bernard S, Salehpour M, Huttner HB, *et al*. Dynamics of hippocampal neurogenesis in adult humans. Cell. 2013; 153: 1219–1227. https://doi.org/10.1016/j.cell.2013.05.002.

[3] Sorrells SF, Paredes MF, Cebrian-Silla A, Sandoval K, Qi D, Kelley KW, *et al*. Human hippocampal neurogenesis drops sharply in children to undetectable levels in adults. Nature. 2018; 555: 377–381. https://doi.org/10.1038/nature25975.

[4] Moreno-Jiménez EP, Terreros-Roncal J, Flor-García M, Rábano A, Llorens-Martín M. Evidences for Adult Hippocampal Neurogenesis in Humans. The Journal of Neuroscience. 2021; 41: 2541–2553. https://doi.org/10.1523/JNEUROSCI.0675-20.2020.

[5] Winner B, Winkler J. Adult neurogenesis in neurodegenerative diseases. Cold Spring Harbor Perspectives in Biology. 2015; 7: a021287. https://doi.org/10.1101/cshperspect.a021287.

[6] Sahay A, Hen R. Adult hippocampal neurogenesis in depression. Nature Neuroscience. 2007; 10: 1110–1115. https://doi.org/10.1038/nn1969.

[7] Lazarov O, Hollands C. Hippocampal neurogenesis: Learning to remember. Progress in Neurobiology. 2016; 138–140: 1–18. https://doi.org/10.1016/j.pneurobio.2015.12.006.

[8] Crews L, Adame A, Patrick C, Delaney A, Pham E, Rockenstein E, *et al*. Increased BMP6 levels in the brains of Alzheimer's disease patients and APP transgenic mice are accompanied by impaired neurogenesis. The Journal of Neuroscience. 2010; 30: 12252–12262. https://doi.org/10.1523/JNEUROSCI.1305-10.2010.

[9] Li Y, Halterman MW. The MAP Kinase Phosphatase MKP-1 Modulates Neurogenesis via Effects on BNIP3 and Autophagy. Biomolecules. 2021; 11: 1871. https://doi.org/10.3390/biom11121871.

[10] Hutchins EJ, Bronner ME. Draxin alters laminin organization during basement membrane remodeling to control cranial neural crest EMT. Developmental Biology. 2019; 446: 151–158. https://doi.org/10.1016/j.ydbio.2018.12.021.

[11] Ahmed G, Shinmyo Y, Ohta K, Islam SM, Hossain M, Naser IB, *et al*. Draxin inhibits axonal outgrowth through the netrin receptor DCC. The Journal of Neuroscience: the Official Journal of the Society for Neuroscience. 2011; 31: 14018–14023. https://doi.org/10.1523/JNEUROSCI.0943-11.2011.

[12] Liu Y, Bhowmick T, Liu Y, Gao X, Mertens HDT, Svergun DI, *et al*. Structural Basis for Draxin-Modulated Axon Guidance and Fasciculation by Netrin-1 through DCC. Neuron. 2018; 97: 1261–1267.e4. https://doi.org/10.1016/j.neuron.2018.02.010.

[13] Hillary RF, McCartney DL, Harris SE, Stevenson AJ, Seeboth A, Zhang Q, *et al*. Genome and epigenome wide studies of neurological protein biomarkers in the Lothian Birth Cohort 1936. Nature Communications. 2019; 10: 3160. https://doi.org/10.1038/s41467-019-11177-x.

[14] Waszczuk MA, Kuan PF, Yang X, Miao J, Kotov R, Luft BJ. Discovery and replication of blood-based proteomic signature of PTSD in 9/11 responders. Translational Psychiatry. 2023; 13: 8. https://doi.org/10.1038/s41398-022-02302-4.

[15] Verstockt B, Verstockt S, Veny M, Dehairs J, Arnauts K, Van Assche G, *et al*. Expression Levels of 4 Genes in Colon Tissue Might Be Used to Predict Which Patients Will Enter Endoscopic Remission After Vedolizumab Therapy for Inflammatory Bowel Diseases. Clinical Gastroenterology and Hepatology. 2020; 18: 1142–1151.e10. https://doi.org/10.1016/j.cgh.2019.08.030.

[16] Jia Y, Liu Z, Cheng X, Liu R, Li P, Kong D, *et al*. DRAXIN as a Novel Diagnostic Marker to Predict the Poor Prognosis of Glioma Patients. Journal of Molecular Neuroscience: MN. 2022; 72: 2136–2149. https://doi.org/10.1007/s12031-022-02054-2.

[17] Zhao J, Zhu Y, Yang J, Li L, Wu H, De Jager PL, *et al*. A genome-wide profiling of brain DNA hydroxymethylation in Alzheimer's disease. Alzheimer's & Dementia: the Journal of the Alzheimer's Association. 2017; 13: 674–688. https://doi.org/10.1016/j.jalz.2016.10.004.

[18] Wu S, Hu L, Fu Y, Chen Y, Hu Z, Li H, *et al*. Effects of Intestinal M Cells on Intestinal Barrier and Neuropathological Properties in an AD Mouse Model. Molecular Neurobiology. 2024; 61: 10006–10022. https://doi.org/10.1007/s12035-023-03807-9.

[19] Kraeuter AK, Guest PC, Sarnyai Z. The Y-Maze for Assessment of Spatial Working and Reference Memory in Mice. Methods in Molecular Biology (Clifton, N.J.). 2019; 1916: 105–111. https://doi.org/10.1007/978-1-4939-8994-2_10.

[20] Islam SM, Shinmyo Y, Okafuji T, Su Y, Naser IB, Ahmed G, *et al*. Draxin, a repulsive guidance protein for spinal cord and forebrain commissures. Science (New York, N.Y.). 2009; 323: 388–393. https://doi.org/10.1126/science.1165187.

[21] Naser IB, Su Y, Islam SM, Shinmyo Y, Zhang S, Ahmed G, *et al*. Analysis of a repulsive axon guidance molecule, draxin, on ventrally directed axon projection in chick early embryonic midbrain. Developmental Biology. 2009; 332: 351–359. https://doi.org/10.1016/j.ydbio.2009.06.004.

[22] Ahmed G, Shinmyo Y, Naser IB, Hossain M, Song X, Tanaka H. Olfactory bulb axonal outgrowth is inhibited by draxin. Biochemical and Biophysical Research Communications. 2010; 398: 730–734. https://doi.org/10.1016/j.bbrc.2010.07.010.

[23] Riyadh MA, Shinmyo Y, Ohta K, Tanaka H. Inhibitory effects of draxin on axonal outgrowth and migration of precerebellar neurons. Biochemical and Biophysical Research Communications. 2014; 449: 169–174. https://doi.org/10.1016/j.bbrc.2014.05.013.

[24] Despres C, Byrne C, Qi H, Cantrelle FX, Huvent I, Chambraud B, *et al*. Identification of the Tau phosphorylation pattern that drives its aggregation. Proceedings of the National Academy of Sciences of the United States of America. 2017; 114: 9080–9085. https://doi.org/10.1073/pnas.1708448114.

[25] Milà-Alomà M, Ashton NJ, Shekari M, Salvadó G, Ortiz-

Romero P, Montoliu-Gaya L, *et al*. Plasma p-tau231 and p-tau217 as state markers of amyloid-β pathology in preclinical Alzheimer's disease. Nature Medicine. 2022; 28: 1797–1801. https://doi.org/10.1038/s41591-022-01925-w.

[26] Miyake A, Takahashi Y, Miwa H, Shimada A, Konishi M, Itoh N. Neucrin is a novel neural-specific secreted antagonist to canonical Wnt signaling. Biochemical and Biophysical Research Communications. 2009; 390: 1051–1055. https://doi.org/10.1016/j.bbrc.2009.10.113.

[27] Fronza MG, Alves D, Praticò D, Savegnago L. The neurobiology and therapeutic potential of multi-targeting β-secretase, glycogen synthase kinase 3β and acetylcholinesterase in Alzheimer's disease. Ageing Research Reviews. 2023; 90: 102033. https://doi.org/10.1016/j.arr.2023.102033.

[28] Zhang X, Heng X, Li T, Li L, Yang D, Zhang X, *et al*. Long-term treatment with lithium alleviates memory deficits and reduces amyloid-β production in an aged Alzheimer's disease transgenic mouse model. Journal of Alzheimer's Disease: JAD. 2011; 24: 739–749. https://doi.org/10.3233/JAD-2011-101875.

[29] Vallée A, Lecarpentier Y, Guillevin R, Vallée JN. Thermodynamics in Neurodegenerative Diseases: Interplay Between Canonical WNT/Beta-Catenin Pathway-PPAR Gamma, Energy Metabolism and Circadian Rhythms. Neuromolecular Medicine. 2018; 20: 174–204. https://doi.org/10.1007/s12017-018-8486-x.

[30] Hübner A, Cavanagh-Kyros J, Rincon M, Flavell RA, Davis RJ. Functional cooperation of the proapoptotic Bcl2 family proteins Bmf and Bim in vivo. Molecular and Cellular Biology. 2010; 30: 98–105. https://doi.org/10.1128/MCB.01155-09.

[31] Zhi Z, Ouyang Z, Ren Y, Cheng Y, Liu P, Wen Y, *et al*. Non-canonical phosphorylation of Bmf by p38 MAPK promotes its apoptotic activity in anoikis. Cell Death and Differentiation. 2022; 29: 323–336. https://doi.org/10.1038/s41418-021-00855-3.

[32] Zhang KR, Zhang YF, Lei HM, Tang YB, Ma CS, Lv QM, *et al*. Targeting AKR1B1 inhibits glutathione de novo synthesis to overcome acquired resistance to EGFR-targeted therapy in lung cancer. Science Translational Medicine. 2021; 13: eabg6428. https://doi.org/10.1126/scitranslmed.abg6428.

[33] Syamprasad NP, Jain S, Rajdev B, Panda SR, Kumar GJ, Shaik KM, *et al*. AKR1B1 drives hyperglycemia-induced metabolic reprogramming in MASLD-associated hepatocellular carcinoma. JHEP Reports: Innovation in Hepatology. 2024; 6: 100974. https://doi.org/10.1016/j.jhepr.2023.100974.

[34] Chau BN, Cheng EH, Kerr DA, Hardwick JM. Aven, a novel inhibitor of caspase activation, binds Bcl-xL and Apaf-1. Molecular Cell. 2000; 6: 31–40.